

# Detecting People Looking at Each Other in Videos

M. J. Marin-Jimenez · A. Zisserman ·  
M. Eichner · V. Ferrari

Received: 5 October 2012 / Accepted: 14 August 2013  
© Springer Science+Business Media New York 2013

**Abstract** The objective of this work is to determine if people are interacting in TV video by detecting whether they are looking at each other or not. We determine both the temporal period of the interaction and also spatially localize the relevant people. We make the following four contributions: (i) head detection with implicit coarse pose information (front, profile, back); (ii) continuous head pose estimation in unconstrained scenarios (TV video) using Gaussian process regression; (iii) propose and evaluate several methods for assessing whether and when pairs of people are looking at each other in a video shot; and (iv) introduce new ground truth annotation for this task, extending the TV human interactions dataset (Patron-Perez et al. 2010). The performance of the methods is evaluated on this dataset, which consists of 300 video clips extracted from TV shows. Despite the variety and difficulty of this video material, our best method obtains an average precision of 87.6 % in a fully automatic manner.

---

M. J. Marin-Jimenez (✉)  
Department of Computing and Numerical Analysis,  
Maimonides Institute for Biomedical Research (IMIBIC),  
University of Cordoba, Cordoba, Spain  
e-mail: mjmarin@uco.es

A. Zisserman  
Department of Engineering Science,  
University of Oxford, Oxford, UK  
e-mail: az@robots.ox.ac.uk

M. Eichner  
ETH Zurich, Zurich, Switzerland  
e-mail: marcin.eichner@vision.ee.ethz.ch

V. Ferrari  
School of Informatics, University of Edinburgh,  
Edinburgh, UK  
e-mail: vferrari@staffmail.ed.ac.uk

**Keywords** Person interactions · Video search ·  
Action recognition · Head pose estimation

## 1 Introduction

If you read any book on film editing or listen to a director's commentary on a DVD, then what emerges again and again is the importance of eyelines. Standard cinematography practice is to first establish which characters are looking at each other using a medium or wide shot, and then edit subsequent close-up shots so that the eyelines match the point of view of the characters. This is the basis of the well known 180° rule in editing.

The objective of this paper is to determine whether eyelines match between characters within a shot—and hence understand which of the characters are interacting. The importance of the eyeline is illustrated by the three examples of Fig. 1—one giving rise to arguably the most famous quote from *Casablanca*, and another being the essence of the humour at that point in an episode of *Fawlty Towers*. Our target application is this type of edited TV video and films. It is very challenging material as there is a wide range of human actors, camera viewpoints and ever present background clutter.

Determining whether characters are interacting using their eyelines is another step towards a fuller video understanding, and complements recent work on automatic character identification (Everingham et al. 2006; Cour et al. 2009; Sivic et al. 2009), human pose estimation (Ferrari et al. 2009; Andriluka et al. 2009; Bourdev et al. 2010; Sapp et al. 2010; Yang et al. 2012), human action recognition (Laptev et al. 2008; Liu et al. 2009; Marín-Jiménez and Pérez de la Blanca 2012; Raptis et al. 2012; Sadanand and Corso 2012), and social (Fathi et al. 2012) and specific interaction recognition (e.g. hugging,



**Fig. 1** Are they looking at each other? Answering this question enables richer video analysis, and retrieval based on where actors interact. From left to right *Friends*, *Casablanca*, *Fawlty Towers*. The eyeline in the *Casablanca* shot gives rise to the famous quote “Here’s looking at you, kid”

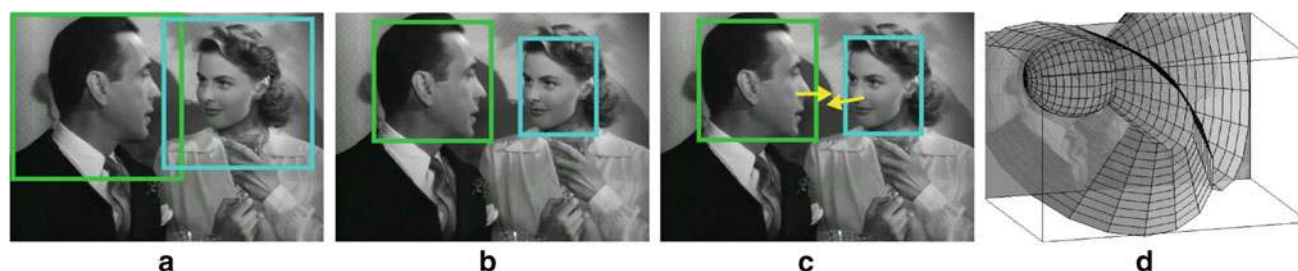


**Fig. 2** Proposed pipeline. **a** Upper-body detection. **b** Head detection inside upper-body areas. **c** Head pose estimation. **d** LAEO scoring between pairs of heads. This example would be correctly classified as LAEO

shaking hands) (Patron-Perez et al. 2012; Yang et al. 2012). Putting interactions together with previous character identification work, it now becomes possible to retrieve shots where two particular actors interact, rather than just shots where the actors are present in the same scene.

In order to determine if two people are looking at each other, it is necessary to detect their head and estimate their head pose. There are two main strands in previous work: 2D approaches, where detectors are built for several aspects of the head [such as frontal and profile Sivic et al. (2009)] or the pose is classified into discrete viewpoints (Tu 2005; Benfold and Reid 2008; Zhu and Ramanan 2012), or regressed (Osadchy et al. 2007). The alternative are 3D approaches, where a 3D model is fitted to the image and hence the pose determined (Blanz and Vetter 2003; Everingham and Zisserman 2005). A survey of head pose estimation is given in Murphy-Chutorian and Trivedi (2009).

In this work, we start by detecting human heads in each video frame separately and then grouping them over time into tracks, each corresponding to a different person. Next, we estimate the *pitch* and *yaw* angles for each head detection. For this, we propose a 2D approach and train a Gaussian process regressor (Rasmussen and Williams 2006) to estimate the head pitch and yaw directly from the image patch within a detection window using publicly available datasets. In the third step, we explore three methods to determine if two people (tracks) are Looking At Each Other (LAEO, Sect. 2). Two people are LAEO if there is eye contact between them. We start with a simple 2D analysis, based on the intersection

of gaze areas in 2D defined by the sign of the estimated yaw angles (Sect. 2.1). In a more sophisticated alternative, we use both the continuous yaw and pitch angles as well as the relative position of the heads (Sect. 2.2). Finally, we propose a ‘2.5D’ analysis, where we use the scale of the detected head to estimate the depth positioning of the actors, and combine it with the full head pose estimate to derive their gaze volumes in 3D (Sect. 2.3). Figure 2 summarizes the proposed pipeline.

We apply these methods (Sect. 5) to the TV human interactions dataset (TVHID) (Patron-Perez et al. 2010). This is very challenging video material with far greater variety in actors, shot editing, viewpoint, locations, lighting and clutter than the typical surveillance videos used previously for classifying interactions (Park and Aggarwal 2004; Ba and Odobez 2009; Waltisberg et al. 2010) where there is a fixed camera and scene. We provide additional ground truth annotation for the dataset, specifying which shots contain people looking at each other. Originally, the dataset only had annotations for four specific interactions (hand-shake, high-five, hugging and kissing) but there are many other shots where people are looking at each other.

In a thorough experimental evaluation on the TVHID, we show that the full head pose estimate (i.e. yaw and pitch angles) in combination with the relative position of the heads in a 3D scenario are needed for most real situations to clearly define if two people are LAEO.

This paper is an extended version of our preliminary work on this subject Marín-Jiménez et al. (2011).

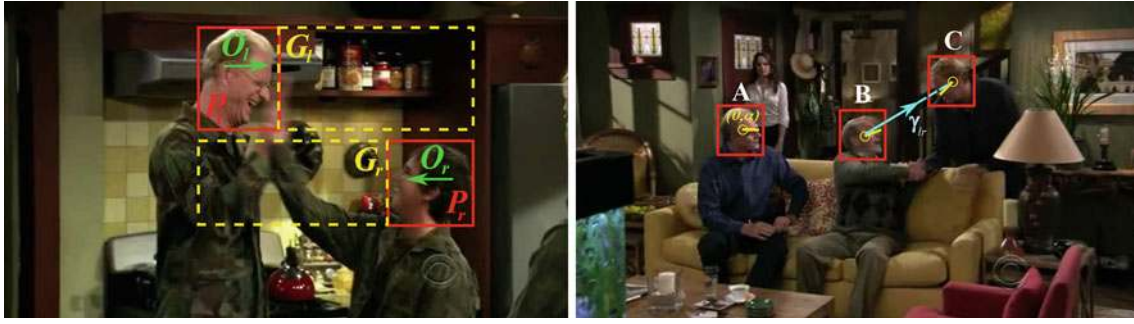


**Fig. 3** *Left: Intersection of gaze areas in 2D.* We show heads ( $P_l$  and  $P_r$ ) as red rectangles and gaze areas ( $G_l$  and  $G_r$ ) as yellow dashed rectangles. The head orientations are represented by green arrows ( $O_l$  and  $O_r$ ). This method would incorrectly say that these people are not LAEO, since their 2D gaze areas do not intersect. *Right: Geometric constraints in 2D.* We show the estimated yaw and pitch angles as yellow

vectors (yaw  $\theta$  determines if left or right facing and length; pitch  $\alpha$  determines orientation). The blue vector  $\gamma_r$  defines the orientation of the vector going from B to C in the image plane. The angle defined by these vectors for (B,C) would classify such pair as LAEO (Color figure online)

## 2 Classifying Pairs of Heads as Looking at Each Other (LAEO)

Let us assume that we know the spatial location of the persons present in a video sequence and we have information about their head orientation as well.

For each person  $i$  in a video frame, let

$$W_i = (x_i, y_i, w_i, h_i, \theta_i, \alpha_i, \sigma_{\theta_i}, \sigma_{\alpha_i})$$

be an image window containing the head, with top-left coordinates  $(x_i, y_i)$ , width  $w_i$ , height  $h_i$ , yaw angle  $\theta_i$  (rotation about  $Y$ -axis), pitch angle  $\alpha_i$  (rotation about  $X$ -axis). The values  $\sigma_{\theta_i}$  and  $\sigma_{\alpha_i}$  represent the uncertainty in the estimate of  $\theta_i$  and  $\alpha_i$ , respectively. Using this information, we propose in this section three methods for classifying a pair of persons as LAEO or not. This is the main contribution of this paper. In Sect. 3 we explain how to perform head pose estimation automatically (i.e. we use Gaussian Process regressors), and in Sect. 4 we explain how to detect and tracks heads (i.e. we build tracks of head detections obtained from previously computed upper-body tracks).

### 2.1 Intersection of Gaze Areas in 2D

The simplest method we propose only considers the head pose as discretized into just two directions, i.e. facing left or right. For this we only use the estimated yaw angle and discard the pitch. In addition to this binary head pose, this method also uses the image position of the head window and its height.

We define as *gaze area*  $G_i$  the image region a person head  $P_i$  is looking at: a horizontal rectangle extending from the head towards the gaze direction (Fig. 3left). The height of  $G_i$  is given by the height of  $P_i$ , while the width is given by the  $x$  position of the farthest other head in the scene. To

classify whether two heads  $P_l, P_r$  are LAEO, we define the  $\text{LAEO}_{GA}(P_l, P_r)$  function. Let  $(x_l, y_l)$  and  $(x_r, y_r)$  be the centres of  $P_l, P_r$ , satisfying the condition  $(x_l \leq x_r)$ , and  $O_l, O_r$  be their orientation (i.e. +1 facing left, -1 facing right). With these definitions,  $\text{LAEO}_{GA}$  is

$$\text{LAEO}_{GA}(P_l, P_r) = \text{IoU}(G_l, G_r) \cdot \delta(O_l \cdot O_r < 0) \quad (1)$$

where  $\text{IoU}(G_i, G_j) = \frac{G_i \cap G_j}{G_i \cup G_j}$  is the intersection-over-union of the heads' gaze areas  $G_i, G_j$  (Fig. 3 left); the Kronecker delta  $\delta(c)$  is 1 if condition  $c$  is true, and 0 otherwise.

### 2.2 Geometric Constraints in 2D

The second method we propose takes into account both the yaw and pitch angles defining the full head pose, as well as the image position of the two heads. Two people are deemed to be LAEO if all the following three conditions are true

- (i) the person on the left has a positive yaw angle and the person on the right has a negative yaw angle
- (ii) the cosine of the difference between their yaw angles is close to -1
- (iii) the vectors defined by the pitch angles are similar to the vectors that join the heads, in both directions.

Figure 3 (right) shows an example that should be highly scored as LAEO.

For a head  $P_i$ , let  $(x_i, y_i)$  be the coordinates of its centre,  $\theta_i, \alpha_i$  the estimated yaw and pitch angles, and  $\sigma_{\theta_i}, \sigma_{\alpha_i}$  the uncertainty associated at each estimated angle, respectively. We define the following function  $\text{LAEO}_{GC}(P_l, P_r)$  to formalize the above constraints and decide if two heads  $P_l, P_r$  are LAEO (with  $(x_l \leq x_r)$ ):

$$\begin{aligned} \text{LAEO}_{GC}(P_l, P_r) \\ = \beta_{\theta} \cdot [\delta(\theta_l \cdot \theta_r < 0 \wedge \theta_l > \theta_r) \cdot (1 - \cos(\theta_l - \theta_r))] \cdot 0.5] \end{aligned}$$

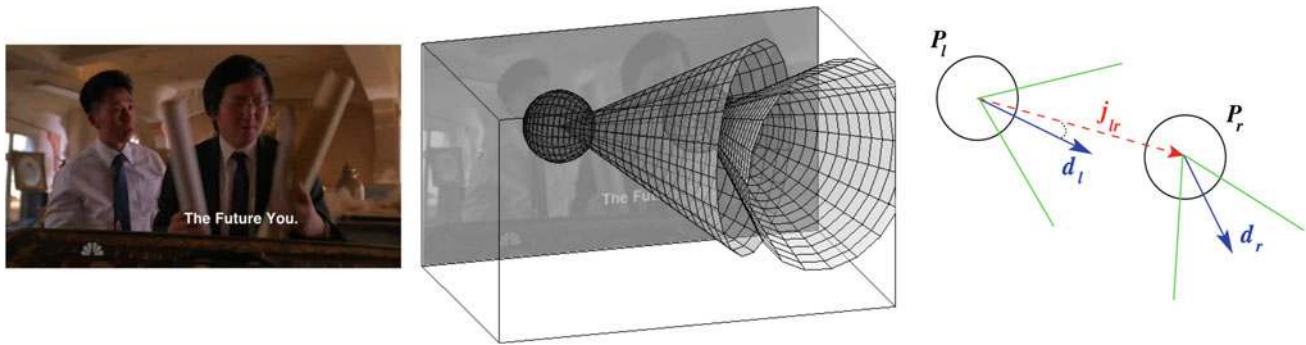


**Fig. 4** Geometric constraints in 3D. (left) Original video frame. (middle) 3D representation of a scene with two people. We show heads (spheres) and their gaze volumes (cones). (right) View from above, with heads (circles) and gaze direction vectors (blue arrows)  $\mathbf{d}_l$  and  $\mathbf{d}_r$  defined by the yaw and pitch angles. Green lines are the boundaries of

the conic gaze volumes. The red vector is  $\mathbf{j}_{lr}$  and goes from  $P_l$  to  $P_r$ . With this configuration,  $P_r$  lays inside  $P_l$  gaze area but  $P_l$  does not lay inside that of  $P_r$ . Therefore, the two people are correctly classified as not LAEO (Color figure online)

$$+ \beta_\alpha \cdot [(1 + \cos(\alpha_l - \gamma_{lr})) \cdot 0.25 + (1 + \cos(\alpha_r - \gamma_{rl})) \cdot 0.25] \quad (2)$$

where  $\gamma_{ij}$  is the orientation of the vector going from  $P_i$  to  $P_j$  in the image plane; the symbol ‘ $-$ ’ between two angles denotes their orientation difference;  $\beta_\theta$  and  $\beta_\alpha$  are weights, so that  $\beta_\theta + \beta_\alpha = 1$ . Note that each row of Eq. (2) (omitting their  $\beta$ ) ranges in  $[0, 1]$ . Therefore,  $\text{LAEO}_{GC}$  ranges in  $[0, 1]$ , with 1 the best possible score.

There are many possible choices for this scoring function, as long as they encode the three conditions stated above. In our case, the first term of Eq. (2) encodes conditions (i) and (ii), based on the yaw angles. The second term encodes condition (iii), based on the pitch angles and the position of the heads.

The weights  $\beta_\theta$  and  $\beta_\alpha$  can be defined as functions of the uncertainties  $\sigma_\theta$  and  $\sigma_\alpha$  associated to the angles  $\theta$  and  $\alpha$ , respectively. These uncertainties are output by the Gaussian Process regressors along with the angle estimates themselves (Sect. 3). Hence, we set  $\beta_\theta$  for a test pair of heads  $P_l, P_r$  as

$$\beta_\theta = (\sigma_{\theta_l}^{-1} + \sigma_{\theta_r}^{-1}) / (\sigma_{\theta_l}^{-1} + \sigma_{\theta_r}^{-1} + \sigma_{\alpha_l}^{-1} + \sigma_{\alpha_r}^{-1}) \quad (3)$$

and  $\beta_\alpha = 1 - \beta_\theta$ . This dynamic weighting gives more weight to reliable estimates of the head orientation, while reducing the negative impact of poor estimates on the LAEO score.

### 2.3 Geometric Constraints in 3D

The most complex method we propose operates in a simplified 3D space. We place each person’s head  $P_i$  in a common 3D coordinate system by using the image coordinates of the head centre as  $(x_i, y_i)$  and deriving the depth coordinate  $z_i$  from the head size in the image. Coordinates  $z_i$  are derived as a direct proportion between all the heads present in the scene, by assuming that in such 3D world all the heads have

the same size and, therefore, the height of the detection window indicates the relative distance of the person to the camera (i.e. larger heads in 2D are closer to the camera than smaller ones). So, heads are  $z$ -ordered so that the largest head in the image is the closest one to the camera. This implicitly assumes that all people have approximately the same head size in the 3D world. This is only a problem in rare cases, i.e. scenes containing both adults and small children, which have significantly different head sizes.

The gaze volume of a head  $P_i$  is represented as a 3D cone  $C_i$  with apex at  $(x_i, y_i, z_i)$  and axis orientation defined by the estimated yaw and pitch angles (Fig. 4). We classify two heads  $P_l$  and  $P_r$  as LAEO if  $P_l$  lays inside  $C_r$ , and  $P_r$  lays inside  $C_l$ . Note how this method uses all the available information.

More formally, we define the  $\text{LAEO}_{3D}$  score by the following equation:

$$\text{LAEO}_{3D}(P_l, P_r) = \frac{(\varphi - \Delta(\mathbf{j}_{lr}, \mathbf{d}_l)) + (\varphi - \Delta(\mathbf{j}_{rl}, \mathbf{d}_r))}{2\varphi} \quad (4)$$

where the angle  $\varphi$  represents the *aperture* of the gaze cone that is a free parameter to be learnt during training (see Sect. 5.3);  $\Delta(\cdot, \cdot)$  is the angle between two vectors;  $\mathbf{d}_i$  is a vector defined by the yaw and pitch angles of  $P_i$ ;  $\mathbf{j}_{lr}$  is the vector from  $P_l$  to  $P_r$ , i.e. defined as  $(x_l, y_l, z_l) \rightarrow (x_r, y_r, z_r)$  (and vice-versa for  $\mathbf{j}_{rl}$ ). Figure 4 illustrates this score. Note how the magnitude of  $\mathbf{d}_i$  is irrelevant, as it is only used inside the  $\Delta$  function.

## 3 Continuous head pose estimation

We describe here our approach to automatically estimate two head pose angles: *yaw* (around the Y axis) and *pitch* (X axis). We do not consider *roll* (Z axis). We use a Gaussian Process





**Fig. 5** Head pose datasets. (top) Samples from CMU-PIE dataset. (bottom) Samples from IDIAP-HP dataset

(GP) to directly regress from the image patch within a head detection window to the two pose angles.

### 3.1 Training a Gaussian Process head pose regressor

For each detected head, we crop an  $N \times N$  image window  $H$  centred on it, where  $N$  is the number of pixels of the largest side of the detection window. Then,  $H$  is resized to a predefined common size  $N' \times N'$ . Given an observed head window  $H$ , the goal is to predict two angles ( $\theta, \alpha$ ) conveying its pose with regard to the camera viewpoint. We formulate this problem in terms of regression, and train two separate regressors, one for yaw ( $\theta$ ) and one for pitch ( $\alpha$ ). As the method is exactly the same, we restrict the explanation to yaw.

The goal is to find a real-valued regression function  $\hat{\theta} = f(g(H))$ , so that  $\hat{\theta} \approx \theta$ , where  $g(H)$  is a feature vector of  $H$ , and  $\theta$  and  $\hat{\theta}$  are the real and estimated angles respectively. We use a histogram of oriented gradients (HOG) [Dalal and Triggs \(2005\)](#) as the head descriptor  $g$ . A HOG descriptor encodes the spatial structure of a rather rigid object through a set of histograms of oriented gradients computed in each cell of a grid overlaid on the window covering the object.

A Gaussian process (GP) ([Rasmussen and Williams 2006](#)) regressor  $f(g(H))$  is employed for estimating the angle. GPs are attractive because they are non-parametric models, and therefore can flexibly adapt to almost any distribution of the data (i.e. provided the mean, covariance and likelihood functions). Moreover, at inference time, they return both the estimate  $\hat{\theta}$  as well as its uncertainty  $\sigma_{\theta}$  (i.e. the mean and variance of the Gaussian posterior). This offers the possibility to downweight uncertain pose estimates in later processing stages (e.g. Sect. 2.2).

### 3.2 Implementation Details and Experimental Validation

A GP ([Rasmussen and Williams 2006](#)) is a collection of random variables, any finite number of which have a joint

Gaussian distribution. A GP is completely specified by its mean function  $m$  and covariance (or kernel) function  $k$ . Given an input vector  $\mathbf{x}$ , the mean function  $m(\mathbf{x})$  and the covariance  $k(\mathbf{x}, \mathbf{x}')$  of a real process  $f(\mathbf{x})$  are defined as

$$m(\mathbf{x}) = E[f(\mathbf{x})], \quad (5)$$

$$k(\mathbf{x}, \mathbf{x}') = E[(f(\mathbf{x}) - m(\mathbf{x}))(f(\mathbf{x}') - m(\mathbf{x}'))] \quad (6)$$

where  $E$  denotes expectation, and  $k(\mathbf{x}, \mathbf{x}')$  indicates that the covariance function is evaluated at the points  $\mathbf{x}$  and  $\mathbf{x}'$ .

Therefore, we write the GP as

$$f(\mathbf{x}) \sim GP(m(\mathbf{x}), k(\mathbf{x}, \mathbf{x}')) \quad (7)$$

where  $f(\mathbf{x})$  is a stochastic function that is distributed as a GP with parameters  $m$  and  $k$ .

We use a linear mean function  $m(\mathbf{x}) = \mathbf{a}\mathbf{x}^T + c$ , where  $\mathbf{a}$  and  $c$  are the *hyperparameters* of  $m$ . We investigate experimentally various functional forms for the covariance  $k$  below.

For making predictions (i.e. computation of the posterior), one also needs to define the functional form of the likelihood function. A common choice is a Gaussian likelihood, since it allows to carry out exact inference ([Rasmussen and Williams 2006](#)).

We use two datasets to learn yaw and pitch angles. The first is the *CMU Pose, Illumination and Expression (CMU-PIE)* dataset ([Sim et al. 2003](#)). It contains images of 68 people from 13 different camera viewpoints, corresponding to 9 discretized yaw angles  $[-90^\circ, 90^\circ]$ . Images have been captured in two different sessions and in each session there are four subsets, corresponding to different types of variations: *expression, illumination, lighting* and *talking*. The top row of Fig. 5 shows some examples of images contained in the dataset.

The second dataset is the *IDIAP head pose (IDIAP-HP)* ([Ba and Odobez 2005](#)). It contains 8 videos recorded in a meeting room and 15 videos in an office. Yaw, pitch and roll angles ground-truth is provided for each person in

**Table 1** RMSE for yaw and pitch

	<i>SEiso</i>	<i>SEisoWN</i>	<i>SEisoPoly</i>	<i>RQiso</i>	<i>Lin</i>
	$\sigma_f^2 \exp\left(-\frac{1}{2l^2}(\mathbf{x}-\mathbf{x}')^T(\mathbf{x}-\mathbf{x}')\right)$	$\sigma_f^2 \exp\left(-\frac{1}{2l^2}(\mathbf{x}-\mathbf{x}')^T(\mathbf{x}-\mathbf{x}')\right) + \sigma_{f'}^2 \delta(\mathbf{x}-\mathbf{x}')$	$\sigma_f^2 \exp\left(-\frac{1}{2l^2}(\mathbf{x}-\mathbf{x}')^T(\mathbf{x}-\mathbf{x}')\right) + \sigma_{f'}^2 (\mathbf{x}^T \mathbf{x}' + c)^3$	$\sigma_f^2 \left(1 + \frac{1}{2al^2}(\mathbf{x}-\mathbf{x}')^T(\mathbf{x}-\mathbf{x}')\right)^{-\alpha}$	$(\mathbf{x}^T \mathbf{x}' + 1)/l^2$
Yaw	<b>15.73</b>	20.42	20.36	20.40	25.86
Pitch	<b>10.09</b>	10.10	10.11	10.16	10.94

Average RMSE performance for various functional forms. The minimum values (i.e. lowest error) for each angle are marked in bold. See main text for discussion

every frame. The bottom row of Fig. 5 shows some examples of cropped frames from videos of the *meeting room* subset. Note that, in contrast to CMU-PIE dataset, people pose diverse pitch angles.

In order to train the head pose estimators, the first step is to detect all the heads from the training images by using the detector of Sect. 4.1. Next, all detected heads are normalized to a common size of  $48 \times 48$  pixels and HOG features are extracted. For computing the HOG descriptor, we use non overlapping cells of  $8 \times 8$  pixels and 9 orientation bins for quantizing the orientation of the gradient vectors. We experimented with other configurations for HOG, but they brought no improvement. Moreover, this configuration is the same as the one used by our head detector, enabling to reuse previous computations. The HOG features are used as input  $\mathbf{x}$  to the GP regressor, which outputs the target angle (i.e.  $\theta$  or  $\alpha$ ). We learn the parameters of the two GP regressors by using the GPML 3.1 library Website (2011a).

We learn the yaw estimator from the subsets *expression* and *illumination* of CMU-PIE dataset, and the pitch estimator from the subset *meeting room* of IDIAP-HP dataset. The set of training data for yaw angle is  $\mathcal{D} = \{(g(H_i), \theta_i)\}$ , where  $g(H_i)$  is the HOG descriptor of the  $i$ -th training sample (i.e. head) and  $\theta_i$  is its ground-truth yaw angle. In order to evaluate the yaw GP regressor, we split the dataset in two parts: six random people are used for validation and the remaining ones for training. We have repeated this procedure for five trials. We measure performance as the root mean squared error (RMSE) averaged over all validation sets, where the error is measured as the difference between the ground-truth angle and the estimated one. We repeat the same procedure for the pitch GP regressor, but using only one for validation in each trial, and all others for training.

We tested various functional forms for the covariance function: diagonal squared exponential (*SEiso*), *SEiso* plus white noise (*SEisoWN*), *SEiso* plus third-order polynomial (*SEisoPoly*), rational quadratic (*RQiso*), and linear with bias (*Lin*). The number of hyperparameters that have to be learned for each covariance function is different: 2 for *SEiso*, 3 for *SEisoWN*, 4 for *SEisoPoly*, 3 for *RQiso* and 1 for *Lin*. Each entry in Table 1 reports the regression performance for a

particular covariance function and angle. Note how *SEiso* leads to the best performance for both angles (yaw and pitch), i.e. 15.73 average RMSE for yaw and 10.09 for pitch. The worst results are delivered by a linear covariance function (i.e. *Lin*).

As a baseline, we trained and validated a linear regressor on the same data (using Matlab's *robustfit* function). This linear regressor has about twice the average RMSE of the GP with *SEiso* covariance. This demonstrates that GP regression is a much better choice than simple linear regression for this task.

After the above evaluations, we chose GP regression with a *SEiso* covariance and we trained a final GP regressor from all the available samples. This final regressor is used in the LAEO experiments (Sect. 5).

#### 4 Detecting and Tracking Heads in Video Shots

We explain here how we detect and track the heads of the people present in a video shot. This is in fact the first step in our processing pipeline. We split the task into the following sub-tasks: (i) human upper-body detection in individual frames; (ii) grouping upper-body detections over time into tracks; (iii) detecting heads within upper-body detection areas; and, (iv) grouping head detections into tracks.

We propose this two-level pipeline because upper-body detection is more robust to clutter than head detection, as it benefits from wider, more distinctive context. The precise localization of the head within the limited area defined by an upper-body detection can then proceed safely. In particular, direct detection of profile heads in uncontrolled scenes would otherwise produce many false positives (Jones and Viola 2003). On the other hand, although we already have tracks in step (ii), another tracking stage is performed in step (iv) in order to resolve situations where two heads are so close that they fall into the same upper-body bounding box (e.g. see Fig. 6, bottom-left).

The detectors are described next, followed by the tracking process in Sect. 4.2.

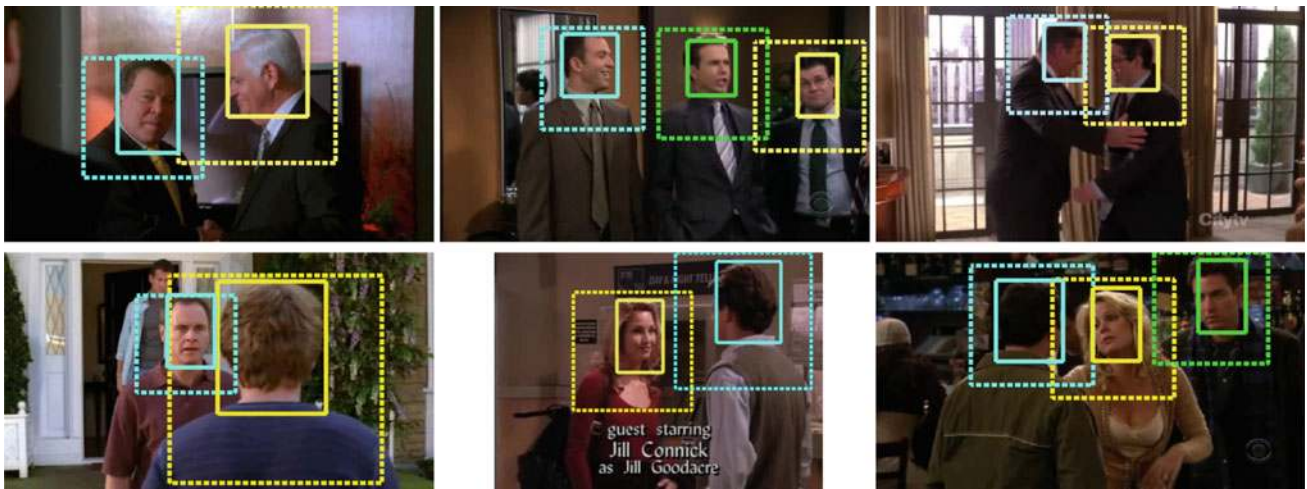


**Fig. 6** Examples of UB (*dashed*) and head (*solid*) detections. The head detector is only run inside UB detection windows. *Note* how heads are localised in various relative positions within the UB windows, adapting to the image content, including *back views*

#### 4.1 Upper-Body and Head Detection

For both the upper-body (UB) and head detectors we use the model of Felzenszwalb et al. (2010), and train using the code released at Website (2010). This code automatically learns the actual components of the detector based on the aspect ratio of the annotated bounding boxes of the positive training samples. However, it is necessary to indicate the number of desired components. In our case, we set one component for the upper-body detector (without a mirror component), two components for the frontal/profile head detector (plus the corresponding mirror ones) and one component for the back-view head detector (plus the mirror one). Figure 7 shows the root filters of the components generated by the learning code.

Figure 6 shows examples of UB and head detections in a variety of situations (i.e. different viewpoints, scales, illumination, clothing, clutter, ...).

##### 4.1.1 Training and Implementation Details

We have used a total of 1,122 annotated video frames from Hollywood movies (Kläser et al. 2010) as positive training

samples for the upper-body detector. These contain upper-bodies viewed from different viewpoints and at different scales. Some examples of UB used during training are shown in Fig. 8 (left). As negative training samples, we used those images in the INRIA-person dataset Website (2005) which do not contain people.

The very same set of Hollywood video frames has been used for training the frontal/profile view components of the head detector. Since the Hollywood movies dataset contains very few back-views of heads, the positive training set for the back-view components of the head detector are manually annotated on 199 video frames extracted from the IDIAP head pose dataset (Ba and Odobez 2005). Some examples of heads used for training are shown in Fig. 8 (right). As this head detector is intended to be run only inside upper-body windows, we provide negative training samples from the area surrounding the head.

#### 4.2 Person Tracking

We describe here the tracker we use to connect over time the single-frame detections produced in the previous stage. The

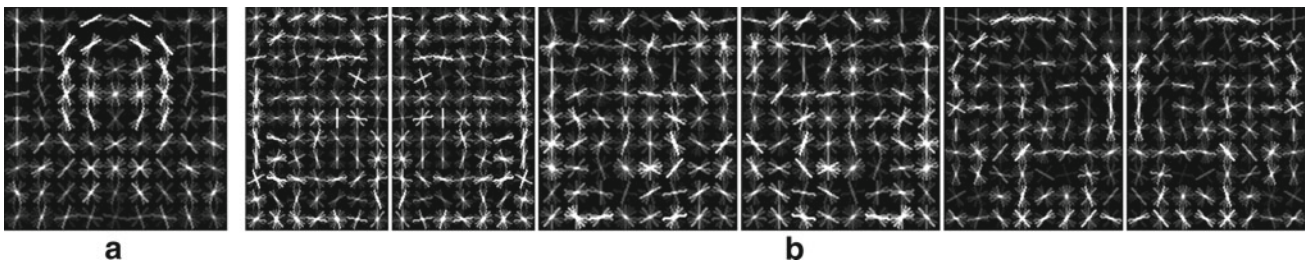


**Fig. 7** Models for the multi-view upper-body and head detectors. **a** Root filter of the UB detector. This model contains a single component trained from a mixture of all viewpoints. **b** Root filters of the 6 com-

ponents of the head detector. Each component provides coarse information about the head orientation. From left to right two near frontal viewpoints, two profile viewpoints and two back viewpoints





**Fig. 8** Examples of samples used for detector training. Left for upper-body detector; right for head detector. Note the variety of poses, people, clothing (in the UB case), and rear of heads

same tracker is used to track upper-body detections or head detections.

For this we design a tracker that combines successful ideas from recent works. As in [Everingham et al. \(2006\)](#), detections in different frames that are connected by many KLT point tracks ([Shi and Tomasi 1994](#)) are more likely to be grouped in the same track. As in [Sivic et al. \(2005\)](#) for faces, we exploit the fact that detections with similar appearance are more likely to be the same person and therefore should be grouped even if far away in time. This helps recovering from full occlusion. Finally, we borrow from [Ferrari et al. \(2008\)](#) the idea of casting the tracking process as a clique partitioning problem. This provides a clear objective function and a well-explored approximate minimization algorithm.

#### 4.2.1 Affinity Measures

More formally, we combine three different kinds of features as cues for grouping: (i) the location of a detection window, (ii) its appearance, and (iii) the motion of point tracks inside it. We measure the affinity between every pair of detections  $D_i, D_j$  in the whole shot according to each of these features.

The location affinity  $W_{loc}(i, j)$  is computed as the area of intersection-over-union between  $D_i$  and  $D_j$ . Note how this takes into account both the position and the scale of the detections. This was the only affinity term used in our previous work [Ferrari et al. \(2008\)](#).

The appearance of each detection is represented by a normalized LAB color histogram. The appearance affinity

between two detections  $D_i, D_j$  is based on the Euclidean distance  $E(i, j)$  between their LAB histograms. The final appearance affinity matrix is  $W_{app}(i, j) = (2 - E(i, j))/2$ .

The last affinity measure counts how many KLT point tracks that pass through  $D_i$  also pass through  $D_j$ . More precisely, let  $S_k$  be the set of KLT tracks passing through a detection  $D_k$ . Then  $W_{klt}(i, j)$  is the intersection-over-union of the sets  $S_i$  and  $S_j$ . Essentially  $W_{klt}(i, j)$  measures ‘how strongly’  $D_i$  and  $D_j$  are connected by point tracks. Figure 9 (right) shows the set of KLT tracks associated to the two UB detections.

This affinity measure is more robust than the location one, as it takes into account the motion inside the detection window. This is especially useful when two persons are close in the image, so that their detection windows overlap (see Fig. 9, right).

#### 4.2.2 Grouping Detections

The three affinity matrices  $W_{loc}, W_{app}, W_{klt}$  are combined into a single matrix  $W_{all}$  as follows

$$W_{all}(i, j) = W_{loc}(i, j) \cdot W_{app}(i, j) \cdot W_{klt}(i, j) \cdot W_{td}(i, j)$$

$$W_{td}(i, j) = \exp(-(|t_i - t_j| - 1)^2 / \sigma_{td}^2) \quad (8)$$

where  $t_i, t_j$  are frame indexes of bounding boxes  $i, j$  and  $W_{td}(i, j)$  is a damping factor limiting similarity to short time difference. We group detections based on  $W_{all}$  using the Clique Partitioning (CP) algorithm of [Ferrari et al. \(2001\)](#), under the constraint that no two detections from the same

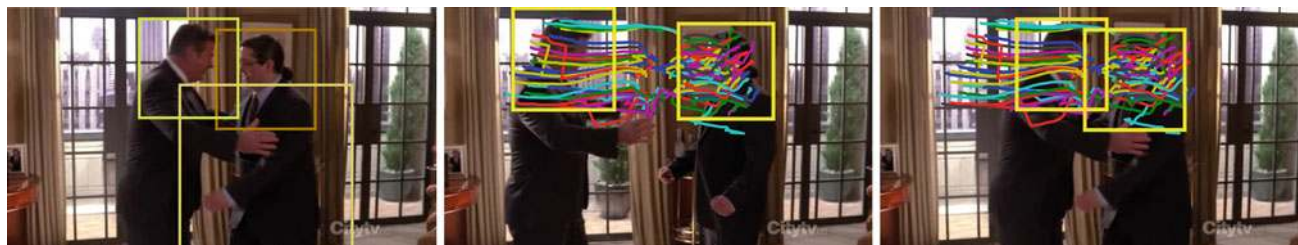


**Fig. 9** Person tracking—motion affinity term. (left) Input upper-body detections in a video frame. (middle, right) KLT point tracks are one of the three cues we use to robustly group detections into tracks



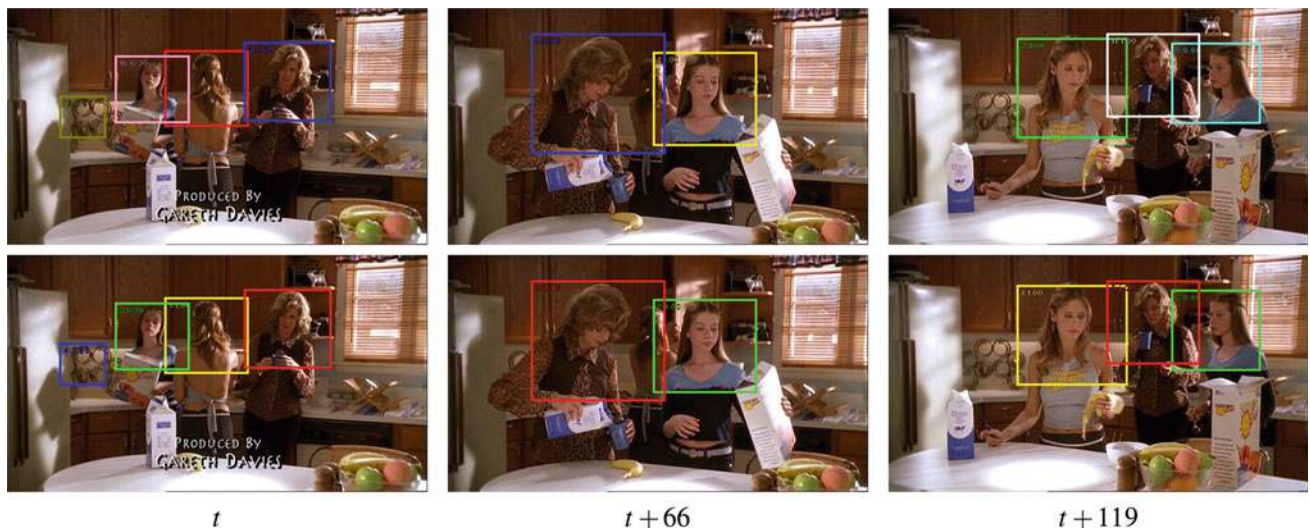


**Fig. 10** Person tracking through full occlusions. Subsequent frames ( $t$ ,  $t + 66$ ,  $t + 119$ ) from a video shot where actors swap positions in the scene. Bounding box colors depict different track IDs. Tracks are

initially broken into multiple tracklets due to full occlusions (*top row*). Connecting tracklets based on appearance similarity enables tracking through full occlusion (*bottom row*)

frame can be grouped. This returns an initial set of tracklets. These tracklets might be interrupted by occlusions, e.g. a person moving behind an occluder would be broken into multiple tracklets (see Fig. 10, top).

In a second stage, tracklets are joined together into full long-term tracks based purely on appearance similarity. We define the similarity between two tracklets as the median appearance similarity  $W_{app}$  between all pairs of frames in the tracklets and group tracklets using CP. This second stage reconnects tracklets belonging to the same person undergoing occlusion (see Fig. 10, bottom).

#### 4.2.3 Post-processing

The process above carefully groups the detections returned by the detector operating in individual frames. However, as the detector is not perfect, it might miss a person in a few frames, even along an otherwise perfect track. In the last stage we fill these ‘holes’ by separate linear interpolation of the window position and size within each tracklet (we assume fixed aspect-ratio of the detection windows). In addition, the position and size values are smoothed over time using a Gaussian filter.

Once the tracking process has finished, false-positive tracks are discarded in a discriminative manner. Inspired by Kläser et al. (2010), we define a feature vector using the following information: number of detections in the track; ratio of number of detections in the track to the shot length; minimum, maximum, average and standard deviation of the detection scores in the track; minimum, maximum, average and standard deviation of the bounding-box width (note that our UB is squared); absolute and relative ranking posi-

tion of track in the shot (based on the sum of the detection scores); and, maximum and average overlap (i.e. intersection-over-union) of the track with the other tracks in the same video shot. Then, we train a linear SVM on these feature vectors. For training purposes, we label a track as positive if it goes through a ground-truth bounding-box in at least one video frame (i.e. overlaps at least 0.5 in terms of intersection-over-union). Otherwise, the track is labelled as negative.

#### 4.3 Performance of People Detection

We evaluate the performance of the UB detector over test data extracted from the *TV human interactions dataset* (TVHID) of Patron-Perez et al. (2010). We evaluate detection rate (DR) versus the average number of false positives per image (FPPI) over all the 27,094 frames that compose the dataset. Following the standard PASCAL VOC protocol (Everingham et al. 2010), we count a detection as correct if the intersection-over-union with any ground-truth bounding-box exceeds 0.5.

Figure 11 reports the performance of our method. The solid green line corresponds to the UBs after tracking, whereas the dashed blue line corresponds to the raw UB detections (i.e. before tracking). The tracker improves DR performance over the whole FPPI range.

Note how our method can handle persons standing close together up to a good degree (see Fig. 6). However, for accurately detecting persons in more extreme cases such as when a person is mostly occluded by the other, a separately trained ‘double person detector’ might be necessary, as proposed by Tang et al. (2012).

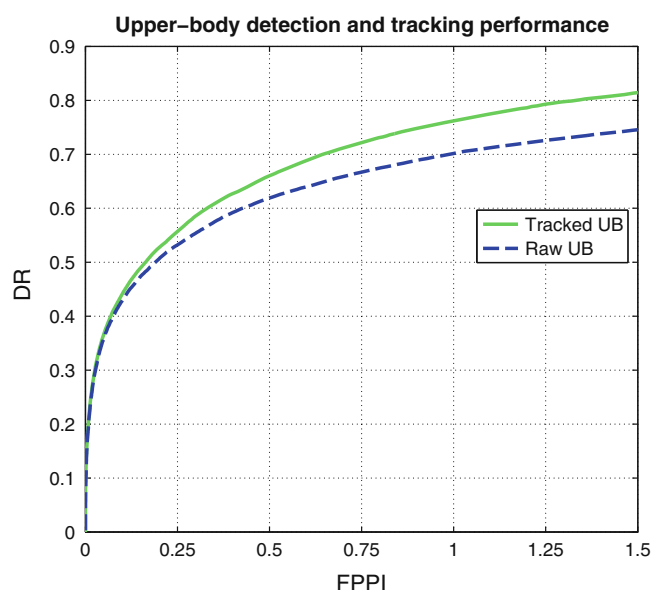


**Fig. 11** Performance of the generic viewpoint upper-body detector and tracker. Detection rate (DR) versus false positives per image (FPPI) are evaluated on the TVHID dataset. The two curves correspond to detecting upper-bodies independently in each frame (blue) and after tracking (green). The latter uses the entire process described in Sect. 4.2, including automatically removing false-positive tracks (Color figure online)

## 5 Experimental Results

### 5.1 LAEO Dataset

We evaluate our LAEO classifiers on the *TV human interactions dataset* (TVHID) of Patron-Perez et al. (2010). It contains a total of 300 video clips grouped in five classes: *hand-shake*, *high-five*, *hug*, *kiss* and *negative*. Each video clip might be composed of several shots, and we detect the shot boundaries as maxima in the colour histogram differences between consecutive frames (Kim and Kim 2009).

For our task, we have provided additional annotation for all the videos by assigning one of the following labels to each shot:

- *label 0* no pairs of people are LAEO
- *label 1* one or more pairs of people are LAEO in a clearly visible manner
- *label 2* a pair of people are LAEO, but at least one of them has occluded eyes (e.g. due to viewpoint or hair)
- *label 3* a pair of people are facing each other, but at least one of them has closed eyes (e.g. during kissing).

There are a total of 443 video shots, where 112 have label 0, 197 label 1, 131 label 2 and 3 label 3. Therefore, the dataset contains 112 negative (label 0) and 331 positive samples (labels 1, 2 and 3). Note that we do not distinguish the three positive labels in the experiments and, for example, we treat

looking at each other with closed eyes as a positive. Figure 12 shows an example for each LAEO label. Both the LAEO annotations and the shot boundaries are available at Website (2011b).

### 5.2 Scoring Pipeline

We evaluate here the performance of the proposed LAEO classifiers on the following task: *is there any pair of people LAEO at any time in this video shot?*

To assign a LAEO score to a shot we apply the following pipeline:

- (i) assign a LAEO score to each pair of people in every frame using one of the methods in Sect. 2. Heads detected by the back-view component are assigned a yaw angle of  $-135^\circ$  or  $+135^\circ$ , depending if they are facing left or right. For the rest of the cases (i.e. frontal/profile head components), the yaw angle returned by the GP regressor is used (i.e. in the range  $[-90^\circ, 90^\circ]$ );
- (ii) assign a LAEO score to each frame, as the maximum over all pairs of people it contains;
- (iii) slide a window along the temporal axis and average the scores of all frames in the window that are greater than a threshold  $T$ ;
- (iv) assign a LAEO score to the shot, as the maximum over all temporal window scores.

Intuitively, these steps will lead to higher scores for pairs of heads that are LAEO over a sustained period of time. This avoids producing false positives for accidental geometric alignments over a few frames (as opposed to simply averaging the thresholded scores over frames). We evaluate performance on the TVHID dataset, using the annotations described above in Sect. 5.1. Each method is used to score every shot, and then the average precision (AP) is used to compare the performance of the methods.

### 5.3 Training-Testing Setup

The TVHID release of Patron-Perez et al. (2010) defines two disjoint partitions. We run experiments on two trials, where one partition is used for training and the other for testing, and then report mean AP (mAP) over the two trials.

We set the free parameters of the proposed LAEO scoring methods so as to maximize AP on the training set, using grid search. These parameters are: (i) the aperture  $\phi$  of the cone in the range  $[15, 45]$  in steps of 5, for the method of Sect. 2.3; (ii) the threshold  $T$  on the LAEO scores used by all methods during the temporal window averaging. We tried  $T$  the range



**Fig. 12** Example LAEO labels. Top-left label 0 (no LAEO). Top-right label 1 (clearly visible LAEO). Bottom-left label 2 (LAEO but with eyes occluded). Bottom-right label 3 (LAEO but with closed eyes). For

our experiments, classes 1, 2 and 3 are considered as positive (green plus symbol), and class 0 as negative (red minus symbol) (Color figure online)

[0.2,0.5] in steps of 0.1; and, (iii) the length of the temporal window  $W$  in the range [5,11] in steps of 2.

#### 5.4 LAEO Baseline

In addition to the three LAEO methods proposed in Sect. 2, we also experiment with a baseline (BL) which, instead of using estimated angles, uses the coarse directional information provided by our head detector (i.e. which model component triggered the detection) to define gaze areas as it in Sect. 2.1. Equation (1) is used to score person pairs. Note that this baseline computes neither yaw nor pitch angles.

#### 5.5 Degrees of Automation

In addition to evaluating the proposed LAEO scoring methods, the experiments evaluate the impact of the different stages of our pipeline by replacing them with ground-truth annotations (for the upper-body detector and for the yaw estimator).

##### 5.5.1 Annotated UBs and Discretized Yaw (GT UB+GT Yaw)

In this experiment we use the ground-truth upper-body annotations included in TVHID to estimate the position of the head. We do the following conversion: given an upper-body

annotation defined by  $(x, y, w, h)$ —top left corner at  $(x, y)$  with width  $w$  and height  $h$ —the estimated head window is computed as  $(x + 0.25 \cdot w, y, 0.6 \cdot w, 0.65 \cdot h)$ . In addition, the annotated head orientation is used as an approximation of the yaw angle. The following five head orientations are possible in the ground-truth: *profile-left*, *frontal-left*, *frontal-right*, *profile-right* and *backwards*. For our experiments, we map such orientations to the following yaw angles in degrees:  $-90$ ,  $-45$ ,  $45$ ,  $90$  and  $180$ . Since information about pitch angle is not annotated, we set it to 0. Note that TVHID does not contain UB annotations in shots where the UB is not fully visible (i.e. face close-ups). We assign a LAEO score of 0 to such shots.

##### 5.5.2 Annotated UBs with Automatic Head Detection and Head Pose Estimation (GT UB+Auto Head)

In this experiment we use the annotated upper-bodies included in TVHID to define the tracks of upper-bodies, as in the previous experiment. But all the rest of the processing is automatic (i.e. head detection and head pose estimation). Note that in this experiment we already use the new back-view head detector during the head detection stage.

##### 5.5.3 Fully Automatic System

This experiment covers the fully automatic system proposed in this work.



We report results for several variants: (i) the system without using the back-view head detector. This corresponds to the results we previously published in [Marín-Jiménez et al. \(2011\)](#) (“Fully auto”); (ii) the system with the new back-view component of the head detector, used to retrieving more heads only (“Fully auto+HB”); (iii) the system using the back-view component to also provide a rough information about the yaw angle of the head, as discussed in Sect. 4.1 (“Fully auto+HB+BA”).

## 5.6 Results

Table 2 summarizes the mAP over the two test sets, once the parameters have been optimized over their respective training sets, for each LAEO method separately. Note that in the experiment “GT UB+GT yaw” the baseline method (BL) is not relevant since the head detector is not used (i.e. the components fired by the head detector are needed by BL, but only the ground truth yaw orientation is used in the referred experiment). For placing results in a proper context, the ratio of positive LAEO over the whole dataset is 0.75, and consequently the chance performance of the system is an AP of 0.75.

Figure 13 shows the precision recall curves of the proposed methods for the test set 2 (top row) and test set 1 (bottom row) by using the fully automatic systems with-

**Table 2** Summary of LAEO experiments

	<i>GA</i>	<i>GC</i>	<i>3D</i>	<i>BL</i>
GT UB+GT yaw	0.869	0.915	0.925	–
GT UB+auto head	0.855	0.893	0.896	0.865
Fully auto ( <a href="#">Marín-Jiménez et al. 2011</a> )	0.822	0.846	0.862	0.816
Fully auto+HB	0.845	0.873	<b>0.876</b>	–
Fully auto+HB+BA	0.841	0.855	0.863	0.842

Each entry corresponds to the average AP over the test sets. *GA* intersection of gaze areas in 2D (Sect. 2.1); *GC* geometric constraints in 2D (Sect. 2.2); *3D* geometric constraints in 3D (Sect. 2.3); *BL* baseline (Sect. 5.4); *HB* head back detector; *BA* backview angle

out ([Marín-Jiménez et al. 2011](#)) (left) and with (right) back-view head detection (“Fully auto+HB”).

### 5.6.1 Discussion

The results reported in Table 2 allow different levels of comparison. We can compare different LAEO scoring methods, keeping the degree of automation and the use of the head-back detector fixed (i.e. compare different values within a row). Comparing BL to GA suggest that using the sign of the estimated yaw angles is roughly equivalent to using the coarse head direction represented by which component

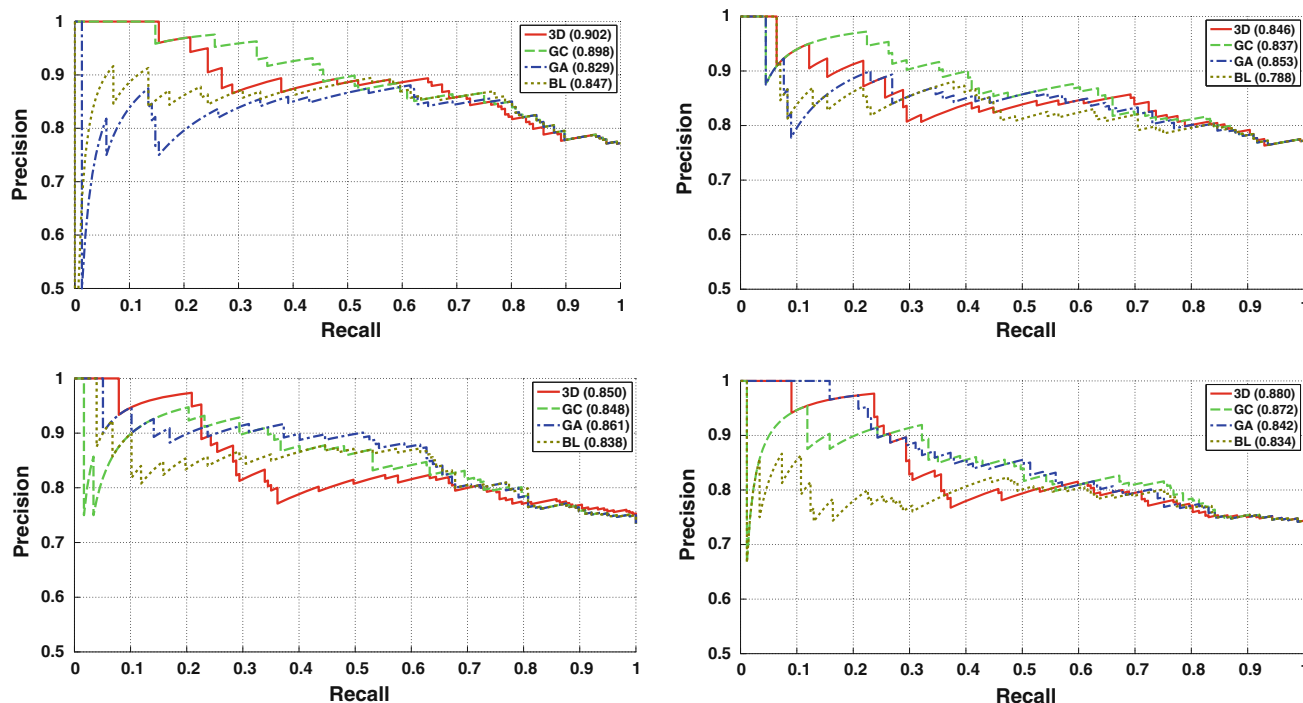
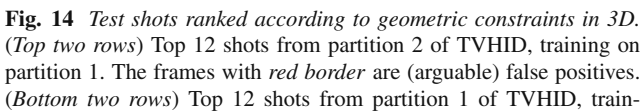


**Fig. 13** Precision recall curves on test sets. (left) Fully automatic system without back-view head detection ([Marín-Jiménez et al. 2011](#)). Top test set 2. Bottom test set 1. (right) Fully automatic system with back-

view head detection (“Fully auto+HB”). Top test set 2. Bottom test set 1. In the legend, the AP of each method is shown in parenthesis



ing on partition 2. *Note* the variety of situations where the proposed method works properly: different scales, poor illumination, cluttered backgrounds, diverse clothing and back-views of people (Color figure online)

 Springer

Finally, comparing “Fully auto+HB” to “Fully auto” (Marín-Jiménez et al. 2011), we can see that mAP is improved for all the LAEO methods. This indicates that detecting back-view heads improves the performance of the system, as it enables more LAEO cases to be covered. However, additionally using the angles associated with the back-view components of the head detector does not further improve the LAEO score, since these angles are very imprecise (“Fully auto+HB+BA”).

In summary, the best mAP that we can achieve with a fully automatic method is **0.876**, which is considerably better than both the baseline and chance levels. Our method is able to localise the LAEO pair both spatially and temporally. Figure 14 shows the middle frame of the highest scored temporal window for each of the top 12 ranked shots, according to 3D LAEO scoring method in experiment “Fully automatic+HB”. Note the variety of scenarios where the method successfully works. Only two arguable false positives are present among those 24 video shots.

## 6 Conclusions

We presented a technique for automatically determining whether people are looking at each other in TV video, including three methods to classify pairs of tracked people. Our best method uses the scale of the detected heads to estimate the depth positioning of the actors, and combines it with the full head pose estimate to derive their gaze volumes in 3D. While we report quantitative performance at shot level, our method allows the interacting people to be localised both spatially (i.e. the pair of heads with the highest LAEO score) and temporally (i.e. temporal sliding window). In conclusion, the recognition of LAEO pairs introduces a new form of high-level reasoning to the broader area of video understanding.

As future work, we plan to study the LAEO problem from the point of view of learning a classifier for LAEO given descriptors over pairs of people as input. For training, this can be cast as a Multiple Instance Learning problem (Dietterich and Lathrop 1997).

**Acknowledgments** We are grateful to the Spanish Minister (projects TIN2012-32952 and BROCA) and for financial support from the Swiss National Science Foundation and ERC Grant VisRec No. 228180. We also thank the reviewers for their helpful comments.

## 7 Appendix: Released Materials

We have released a variety of output from the research that led to this paper:

- (i) the video shot decomposition Website (2011b) of the TVHID videos;

- (ii) the LAEO annotations Website (2011b) on TVHID used in our experiments; and,
- (iii) the head detector Website (2011c) trained to deal with different viewpoints.

## References

- Andriluka, M., Roth, S., & Schiele, B. (2009). Pictorial structures revisited: People detection and articulated pose estimation. In *Proceedings of the IEEE Conference on Computer Vision and Pattern Recognition*.
- Ba, S., & Odobez, J. M. (2005). Evaluation of multiple cue head pose estimation algorithms in natural environments. In *Proceedings of the IEEE International Conference on Multimedia and Expo*.
- Ba, S., & Odobez, J. M. (2009). Recognizing visual focus of attention from head pose in natural meetings. *IEEE Transactions on Systems, Man, and Cybernetics, Part B: Cybernetics*, 39(1), 16–33.
- Benfold, B., & Reid, I. (2008). Colour invariant head pose classification in low resolution video. In *Proceedings of the British Machine Vision Conference*.
- Blanz, V., & Vetter, T. (2003). Face recognition based on fitting a 3d morphable model. *IEEE Transactions on Pattern Analysis and Machine Intelligence*, 25, 1063–1074.
- Bourdev, L., Maji, S., Brox, T., & Malik, J. (2010). Detecting people using mutually consistent poselet activations. In *Proceedings of the European Conference on Computer Vision*.
- Cour, T., Sapp, B., Jordan, C., & Taskar, B. (2009). Learning from ambiguously labeled images. In *Proceedings of the IEEE Conference on Computer Vision and Pattern Recognition*.
- Dalal, N., & Triggs, B. (2005). Histogram of Oriented Gradients for Human Detection. In *Proceedings of the IEEE Conference on Computer Vision and Pattern Recognition*, vol.2, (pp. 886–893).
- Dietterich, T. G., Lathrop, R. H., & Lozano-Pérez, T. (1997). Solving the multiple instance problem with axis-parallel rectangles. *Artificial Intelligence*, 89(12), 31–71.
- Everingham, M., & Zisserman, A. (2005). Identifying individuals in video by combining generative and discriminative head models. In *Proceedings of the International Conference on Computer Vision*.
- Everingham, M., Sivic, J., & Zisserman, A. (2006). Hello! My name is... Buffy: Automatic naming of characters in TV video. In *Proceedings of the British Machine Vision Conference*.
- Everingham, M., Van Gool, L., Williams, C. K. I., Winn, J., & Zisserman, A. (2010). The pascal visual object classes (voc) challenge. *International Journal of Computer Vision*, 88(2), 303–338.
- Fathi, A., Hodgins, J., & Regh, J. (2012). Social interactions: A first-person perspective. In *Proceedings of the IEEE Conference on Computer Vision and Pattern Recognition*.
- Felzenszwalb, P., Girshick, R., McAllester, D., & Ramanan, D. (2010). Object detection with discriminatively trained part based models. *IEEE Transactions on Pattern Analysis and Machine Intelligence*, 32(9), 1627–1645.
- Ferrari, V., Tuytelaars, T., & Van Gool, L. (2001). Real-time affine region tracking and coplanargrouping. In *Proceedings of the IEEE Conference on Computer Vision and Pattern Recognition*.
- Ferrari, V., Marin, M., & Zisserman, A. (2008). Progressive search space reduction for human pose estimation. In *Proceedings of the IEEE Conference on Computer Vision and Pattern Recognition*.
- Ferrari, V., Marin-Jimenez, M., & Zisserman, A. (2009). Pose search: Retrieving people using their pose. In *Proceedings of the IEEE Conference on Computer Vision and Pattern Recognition*.
- Jones, M., & Viola, P. (2003). Fast multi-view face detection. Technical Report TR2003-96, MERL.



- Kim, W. H., & Kim, J. N. (2009). An adaptive shot change detection algorithm using an average of absolute difference histogram within extension sliding window. In *IEEE International Symposium on Consumer Electronics*.
- Kläser, A., Marszałek, M., Schmid, C., & Zisserman, A. (2010). *Human focused action localization in video* (pp. 219–233). ECCV-International Workshop on Sign, Gesture, Activity.
- Laptev, I., Marszałek, M., Schmid, C., & Rozenfeld, B. (2008). Learning realistic human actions from movies. In *Proceedings of the IEEE Conference on Computer Vision and Pattern Recognition*.
- Liu, J., Luo, J., & Shah, M. (2009). Recognizing realistic actions from videos. In *Proceedings of the IEEE Conference on Computer Vision and Pattern Recognition*.
- Marín-Jiménez, M., Zisserman, A., & Ferrari, V. (2011). Here's looking at you kid. Detecting people looking at each other in videos. In *Proceedings of the British Machine Vision Conference*.
- Marín-Jiménez, M., Pérez de la Blanca, N., & Mendoza, M. (2012). Human action recognition from simple feature pooling. *Pattern Analysis and Applications*.
- Murphy-Chutorian, E., & Trivedi, M. M. (2009). Head pose estimation in computer vision: A survey. *IEEE Transactions on Pattern Analysis and Machine Intelligence*, 31, 607–626.
- Osadchy, M., Cun, Y., & Miller, M. (2007). Synergistic face detection and pose estimation with energy-based models. *Journal of Machine Learning Research*, 8, 1197–1215.
- Park, S., & Aggarwal, J. (2004). A hierarchical bayesian network for event recognition of human actions and interactions. *Association For Computing Machinery Multimedia Systems Journal*.
- Patron-Perez, A., Marszałek, M., Reid, I., & Zisserman, A. (2010). High Five: Recognising human interactions in TV shows. In *Proceedings of the British Machine Vision Conference*.
- Patron-Perez, A., Marszałek, M., Reid, I., & Zisserman, A. (2012). Structured learning of human interactions in tv shows. *IEEE Transactions on Pattern Analysis and Machine Intelligence*, 34(12), 2441–2453.
- Raptis, M., Kokkinos, I., & Soatto, S. (2012). Discovering discriminative action parts from mid-level video representations. In *Proceedings of the IEEE Conference on Computer Vision and Pattern Recognition*.
- Rasmussen, C. E., & Williams, C. K. I. (2006). *Gaussian processes for machine learning*. Cambridge, MA: MIT Press.
- Sadanand, S., & Corso, J. (2012). Action bank: A high-level representation of activity in video. In *Proceedings of the IEEE Conference on Computer Vision and Pattern Recognition*.
- Sapp, B., Toshev, A., & Taskar, B. (2010). Cascaded models for articulated pose estimation. In *Proceedings of the European Conference on Computer Vision*.
- Shi, J., & Tomasi, C. (1994). Good features to track (pp. 593–600). In *Proceedings of the IEEE Conference on Computer Vision and Pattern Recognition*.
- Sim, T., Baker, S., & Bsat, M. (2003). The CMU pose, illumination, and expression database. *IEEE Transactions on Pattern Analysis and Machine Intelligence*, 25(1), 1615–1618.
- Sivic, J., Everingham, M., & Zisserman, A. (2005). Person spotting: Video shot retrieval for face sets. In *Proceedings of the ACM International Conference on Image and Video Retrieval*.
- Sivic, J., Everingham, M., & Zisserman, A. (2009). “Who are you?”: Learning person specific classifiers from video. In *Proceedings of the IEEE Conference on Computer Vision and Pattern Recognition*.
- Tang, S., Andriluka, M., & Schiele, B. (2012). Detection and tracking of occluded people. In *Proceedings of the British Machine Vision Conference*.
- Tu, Z. (2005). Probabilistic boosting-tree: Learning discriminative models for classification, recognition, and clustering. In *Proceedings of the International Conference on Computer Vision*.
- Waltisberg, W., Yao, A., Gall, J., Gool, L.V. (2010). Variations of a Hough-voting action recognition system. In *Proceedings of the International Conference on Pattern Recognition (ICPR) 2010 Contests*.
- Website. (2005). INRIA person dataset. <http://pascal.inrialpes.fr/data/human/>.
- Website. (2010). Deformable parts model code. <http://www.cs.brown.edu/pff/latent/>.
- Website. (2011a). GPML Matlab code. <http://www.gaussianprocess.org/gpml/code/matlab/doc/>.
- Website. (2011b). LAEO annotations. <http://www.robots.ox.ac.uk/vgg/data/laeo/>.
- Website. (2011c). LAEO project. <http://www.robots.ox.ac.uk/vgg/research/laeo/>.
- Yang, Y., Baker, S., Kannan, A., & Ramanan, D. (2012). Recognizing proxemics in personal photos. In *Proceedings of the IEEE Conference on Computer Vision and Pattern Recognition*.
- Zhu, X., & Ramanan, D. (2012). Face detection, pose estimation and landmark localization in the wild. In *Proceedings of the IEEE Conference on Computer Vision and Pattern Recognition*.